S5P/TROPOMI TOTAL BrO ALGORITHM TCBRO

ALGORITHM THEORETICAL BASIS DOCUMENT

document number: S5P- BIRA-L2-TCBRO- ATBD
CI identification : TBD
issue : 1.2.0
processor version : 1.2.3
date : 2023-12 23
status : Draft

Document approval record

	digital signature
prepared:	Jeroen van Gent
Checked:	Sander Niemeijer, ….
approved PI:	
approved PM:	

Document change record

issue	date	item	comments
0.1.0	2020-07-24	All	Initial draft version
1.0.0	2022-01-12	All	First full version
1.1.0	2022-06-17	All	Minor text corrections.
1.2.0	2023-12-24	Section 2.4 Section 6.1	Added reference to Atmosphere Virtual Lab New computational effort estimates, in accordance to processor upgrade v1.2.3.

Contents

List of figures

List of tables

List of items to be done (TBD):

TBD: Perform sensitivity study into the validity of the geometric approach for the AMF over different scene types.

TBD: Perform sensitivity tests on satellite data to estimate systematic contributions to the slant column uncertainty.

1 Introduction

1.1 Identification

This document describes the prototype algorithm TCBRO for the retrieval of total vertical bromine monoxide columns from TROPOMI measurements in the UV part of the spectrum.
The algorithm was developed in the frame of the ESA-funded project S5P-PAL (S5P Product Algorithm Laboratory), lead by S&T.
In part, the algorithm was meant to test the functionality of the S5P-PAL as a development and testing working environment for new S5P L2 products. It is now foreseen that the TCBRO scheme, along with its auxiliary processor BGBRO, will be implemented in a pre-operational execution environment in the next few months.

1.2 Purpose and objective

The purpose of the document is to give a high-level description of the algorithm that is used to retrieve total vertical bromine monoxide columns from TROPOMI measurements, the necessary input and auxiliary data, and the output that is generated. In addition, information about the size of the product, calculation times, and the accuracy are provided.

1.3 Document overview

Chapter 4 gives a brief introduction to bromine monoxide retrieval. Chapter 5 provides a high level description of the retrieval algorithm. In Chapter 6 validation and tools for validation are discussed. In Chapter 7, conclusions are drawn. A description of the TROPOMI instrument and performance, referred to from all S5-P/TROPOMI ATBDs, can be found in RD14.

1.4 Acknowledgements

The authors would like to thank the following people for useful discussions, information and other contributions: Sora Seo of DLR and Andreas Richter of IUP Bremen

2 Applicable and reference documents

2.1 Applicable documents

[AD01] GMES Sentinel-5 Precursor – S5P System Requirement Document (SRD); source: ESA/ESTEC; ref: S5P-RS-ESA-SY-0002; issue: 4.1; date: 2011-04-29

[AD02] Sentinel-5P Level 2 Processor Development – Statement of Work -; source: ESA; ref: S5P-SW-ESA-GS-053; issue: 1.1; date: 2012-05-21

[AD03] S5P Level 2 Processor Development – Level 2 Processor Requirements Specifications source: ESA; ref: S5P-SW-ESA-GS-054; issue 1.2 draft; date: 2014-09-15

[AD04] S5P/TROPOMI Level 2 Product Development Plan, source: KNMI, ref: S5P-KNMI-L2CO-0010-PL issue: 1.1.0 date: 2014-06-02

[AD05] S5P – Tailoring of ECSS Standards for the Level 2 Processor Development; source: ESA; ref: SP-RS-ESA-GS-055; issue 1.1dr; date: 2012-10-31

[AD06] Sentinel-5P Level 2 Processor Development: Coordination Tasks; source: ESA; ref: S5P-SW-ESA-GS-081; issue: 1; date: 2012-06-27

2.2 Standard documents

There are no standard documents

2.3 Reference documents

[RD01] Terms, definitions and abbreviations for TROPOMI L01b data processor; source: KNMI; ref: S5P-KNMI-L01B-0004-LI; issue: 3.0.0; date: 2013-11-08

[RD02] Terms, and symbols in the TROPOMI Algorithm Team; source: KNMI; ref: SN-TROPOMI-KNMI-L2-049-MA; issue: 1.0.0; date: 2015-07-16

[RD03] Science Requirements Document for TROPOMI. Volume 1; source: KNMI & SRON; ref: RS-TROPOMI-KNMI-017; issue: 2.0; date: 2008-10-30.

[RD04] GMES Sentinels-4 and-5 Mission Requirements Document (MRD); source: ESA; ref: EO-SMA-/1507/JL; issue: 3; date: 2011-09-21

[RD05] Report Of The Review Of User Requirements For Sentinels-4/-5; source: ESA; ref: EO-SMA-/1507/JL; issue: 2.1; date: 2011-12-21

[RD06] CAPACITY: Operational Atmospheric Chemistry Monitoring Missions – Final report; source: KNMI; ref: CAPACITY; date: Oct. 2005.

[RD07] CAMELOT: Observation Techniques and Mission Concepts for Atmospheric Chemistry; source: KNMI; ref: RP-CAM-KNMI-050; date: Nov. 2009.

[RD08] TRAQ: Performance Analysis and Requirements Consolidation - Final Report; source: KNMI; ref: RP-ONTRAQ-KNMI-051; date: Jan. 2010.

[RD09] S5P/TROPOMI ATBD of the Aerosol data products; source: KNMI; ref: S5P-KNMI-L2-0008-RP-TROPOMI_ATBD_UVAI; issue: 1.1.0; date: 2018-06-15.

[RD10] S5P/TROPOMI ATBD of the Cloud data products; source: DLR; ref: S5P-L2-DLR-ATBD-400I_Clouds; issue: 2.2.0; date: 2020-06-15.

[RD11] S5P/TROPOMI ATBD of the total and tropospheric NO2 data products; source: KNMI; ref: S5P-KNMI-L2-0005-RP-ATBD_NO2_data_products; issue: 1.4.0; date: 2019-02-06.

[RD12] S5P/TROPOMI ATBD of the SO_2 data products; source: BIRA-IASB; ref: S5P-L2- BIRA-ATBD-SO2-400E; issue: 2.2.0; date: 2020-06-15.

[RD13] S5P/TROPOMI Static input for Level 2 processors; source: KNMI; ref: S5P-KNMI-L2CO-0004-SD; issue: 3.0.0; date: 2015-02-27.

[RD14] TROPOMI Instrument and Performance Overview; source: KNMI; ref: S5P-KNMI-L2-0010-RP; issue: 0.10.0; date: 2014-03-15.

[RD15] Sentinel-5 Precursor Level 2 UPAS Processor Input / Output Definition Document; source: DLR; ref: S5P-L2-DLR-IODD-3002; issue: 3.5.0; date: 2019-08-09.

[RD16] Sentinel-5 precursor/TROPOMI Level 2 Product User Manual Formaldehyde HCHO; source: DLR; ref: S5P-L2-DLR-PUM-400F; issue: 2.2.0; date: 2020-06-15.

[RD17] Quarterly Validation Report of the Copernicus Sentinel-5 Precursor Operational Data Products; ref: S5P-MPC-IASB-ROCVR; issue: 6.0.1; date: 2020-03-30.

[RD18] S5-P/TROPOMI Total BrO algorithm TCBRO: validation report, source: BIRA_IASB; ref: S5P-BIRA-L2-VR-TCBRO, issue: 1.0.0, date: 2022-01-09.

[RD19] S5-P/TROPOMI TCBRO and its auxiliary processor BGBRO Input/Output Definition Document, source: BIRA-IASB, ref: S5P- BIRA-L2-IODD-TCBRO, issue: 1.2.0, date: 2023-12-23.

[RD20] S5-P/TROPOMI TCBRO and its auxiliary processor BGBRO Product User Manual, source: BIRA-IASB, ref: S5P- BIRA-L2-PUM-TCBRO, issue: 1.2.0, date: 2023-12-23.

[RD21] S5-P/TROPOMI L2 Product Format Specification for the offline Total Bromine Monoxide algorithm TCBRO and its auxiliary algorithm BGBRO, source: BIRA-IASB, ref: S5P- BIRA-L2-PFS-TCBRO, issue: 1.2.0, date: 2023-12-23.

2.4 Electronic references

[URL01] http://uv-vis.aeronomie.be/software/QDOAS/

[URL02] http://uv-vis.aeronomie.be/software/QDOAS/QDOAS_manual.pdf

[URL03] https://atmospherictoolbox.org/

[URL04] https://atmosphere virtuallab.org/

[URL05] https://www.s5p-pal.com/

3 Terms, definitions and abbreviated terms

Terms, definitions and abbreviated terms that are used in the development program for the TROPOMI L0-1b data processor are described in [RD01]. Terms, definitions and abbreviated terms that are used in the development program for the TROPOMI L2 data processors are described in [RD02]. Terms, definitions and abbreviated terms that are specific for this document can be found below.

3.1 Terms and definitions

The most important symbols related to the data product described in this document – some of which are not in [RD02]– are the following:

AK	averaging kernel
m	altitude-resolved air mass factor or weighting function
M	air-mass factor
M^{geo}	geometric air-mass factor
N_s	slant column density
N_v	vertical column density

3.2 Acronyms and abbreviations

AAI	Absorbing Aerosol Index
AMF	Air Mass Factor
BrO	Bromine Monoxide
BIRA	Belgian Institure for Space Aeronomy
BRDF	Bidirectional reflectance distribution function
CH_4	Methane
CO	Carbon Monoxide
CRB	Clouds as Reflecting Boundaries
CTM	Chemistry Transport Model
DOAS	Differential Optical Absorption Spectroscopy
ENVISAT	Environmental Satellite
ERS	European Remote Sensing satellite
FRESCO	Fast Retrieval Scheme for Clouds from the Oxygen A band
GOME-2	Global Ozone Monitoring Experiment–2
HCHO	Formaldehyde
LOS	Line Of Sight

MAG	Mission Advisory Group
MetOp	Meteorological Operational Satellite
NMVOC	Non-Methane Volatile Organic Compound
NO_x	Nitrogen oxides
NRT	near-real time (i.e. processing within 3 hours of measurement)
OCRA	Optical Cloud Recognition Algorithm
OE	Optimal Estimation
OMI	Ozone Monitoring Instrument
O_3	Ozone
PDGS	Sentinel-5 Precursor Payload Data Ground Segment (at DLR)
RAA	Relative Azimuth Angle
ROCINN	Retrieval of Cloud Information using Neural Networks
SCIAMACHY	Scanning Imaging Absorption spectroMeter for Atmospheric Cartography
S5P-PAL	Sentinel-5P Product Algorithm Laboratory
SZA	Solar Zenith Angle
TROPOMI	Tropospheric Monitoring Instrument
VOC	Volatile Organic Compound
VZA	Viewing Zenith Angle

4 BrO Retrieval from S5-P/TROPOMI.

4.1 TROPOMI

The TROPOsphere monitoring Instrument aboard the Copernicus Sentinel-5 Precursor (S5-P) satellite mission is a hyperspectral imager detecting backscattered radiance with a spectral range from the ultraviolet to the shortwave infrared. Its polar orbit and 2600 wide swath assure almost full global coverage every day. TROPOMI's spatial resolution is unprecedented, with ground footprint sizes as small as 3.5×7 km^2 and even 3.5×5.5 km^2 since 6 August 2019; this allows for the monitoring of atmospheric trace gas distributions with finer detail than ever before.
An extensive description of the instrument and its measurement procedures can be found in RD14.

4.2 Satellite retrieval of atmospheric BrO

Inorganic bromine (Bry =Br+BrO+BrONO2 +HOBr+HBr +BrCl) plays an important role in the chemistry of the stratosphere. Bromine monoxide (BrO) contributes to mid-latitude ozone loss by about 25% and to polar ozone depletion, mostly through the BrO/ClO cycle (McElroy et al., 1986), up to 50%.The main sources of Bry in the stratosphere are long-lived organic bromine compounds (CH3Br, CBrClF2, CBrF3, CBrF2CBrF2), mostly of anthropogenic origin, but additional contributions must be considered, possibly due to the release from short-lived biogenic organic compounds (e.g., CHBr3, CH2Br2) or even through direct injection of tropospheric Bry into the lower stratosphere (WMO, 2018).
Inorganic bromine has also a significant effect in the troposphere. Every polar spring, BrO is released to the troposphere over sea ice covered regions through a series of heterogeneous photochemical reactions (see e.g. Simpson et al., 2007 and Figure 1). This mechanism depletes boundary layer and tropopsheric ozone, changes the oxidizing capacity of the atmosphere and facilitates the deposition of mercury into wild ecosystems. On a more local scale, BrO has been identified over salt lakes (Hebestreit et al.,1999) and in volcanic plumes (Bobrowski et al., 2003). Also, a variety of observations have shown that inorganic bromine may be produced and sustained in the free troposphere at the global scale.
In order to understand and monitor the evolution of atmospheric bromine and its interaction with a changing climate, satellite UV-visible remote sensing observations of BrO have been developed and refined over the last two decades, as they offer the unique capability to study and monitor BrO at the global scale (Chance, 1998; Richter et al., 1998, 2002; Van Roozendael et al., 2002; Wagner and Platt, 1998, Theys et al., 2009; Theys et al., 2011; Sihler et al., 2012; Choi et al., 2018; Seo et al., 2019). With the advent of new high spatial resolution sensors like Sentinel-5P/TROPOMI and the future EPS-SG/Sentinel-5, the understanding of bromine emissions and related impact on atmospheric chemistry is expected to improve in the future.

Remote sensing measurements of BrO are generally performed by applying Differential Optical Absorption Spectroscopy (DOAS, Platt & Stutz, 2008) in the 319 – 364 nm spectral region where the molecule exhibits characteristic absorption structures. The retrieved quantity from the spectral fit is a slant column, representing the total BrO denity along the integrated lightpath. This slant column is subsequently converted into a vertical column amount by means of an air mass factor.

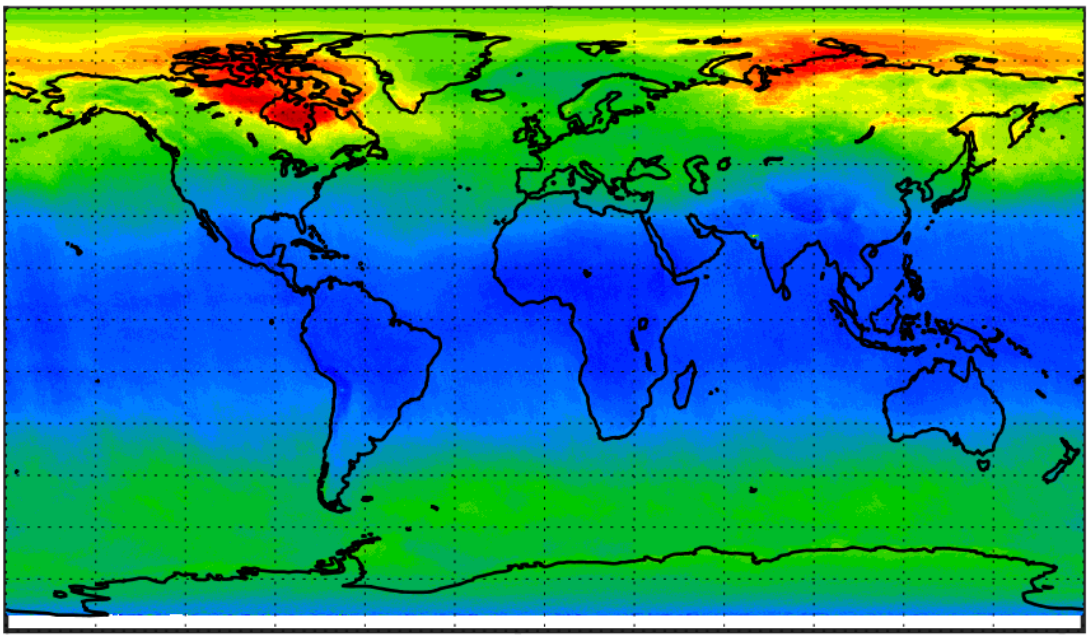

Figure 1: Example of S5P/TROPOMI total vertical BrO columns retrieved by TCBRO (monthly-averaged signal for April 2019.

5 The bromine monoxide retrieval algorithm TCBRO

5.1 Algorithm description

Figure 1 shows the full flow diagram of the BrO retrieval algorithm including the dependencies on auxiliary data.
In brief, the BrO vertical column densities (*Nv*) are retrieved using a residual technique (Theys et al., 2011) according to the following equation:

$$N_v = \frac{N_s - N_{s,0}}{M} \qquad 5\text{-}1$$

The approach consists of three main steps:
1. A slant column density (N_v) is determined from calibrated earth-shine and radiance or irradiance reference spectra using a DOAS fit, as further explained in Sect. 5.2.1. This slant column is a "total" SCD in the sense that it includes contributions from absorption by BrO in both the stratosphere and troposphere. To correct for possible stripes and offsets in the data a correction $N_{s,0}$ of the data is implemented (Section 5.2.2)
2. The total vertical column (N_v) is estimated using an air mass factor M.

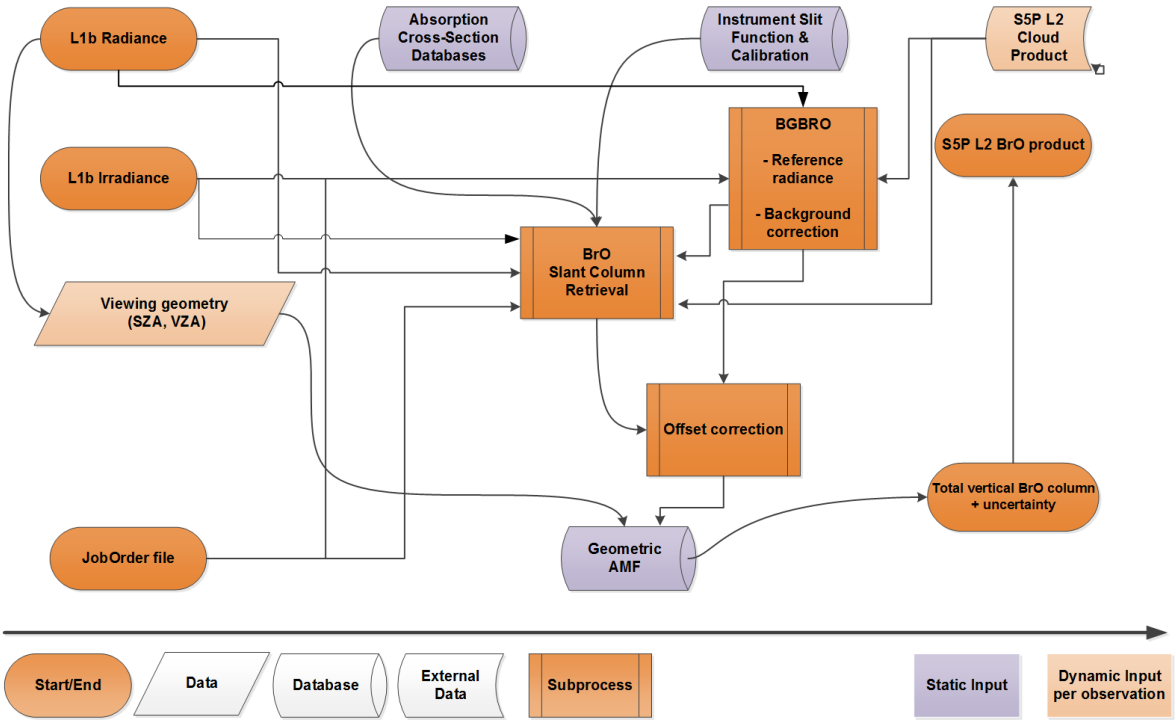

Figure 2: Flow diagram of the S5-P BrO retrieval algorithm. The BGBRO module for the calculation of parameters for radiance-as-reference and background correction is in reality an independent processor.

The slant column fitting procedure is performed by the QDOAS software component, developed and maintained at BIRA-IASB ([URL01], [URL02], Fayt & Van Roozendael, 2001, Danckaert et al., 2012). QDOAS is also one of the four building blocks of the ESA Atmospheric Toolbox/Virtual Lab ([URL03], [URL04]).

5.1.1 DOAS slant column fitting

Error! Reference source not found. sketches the geometry of a nadir satellite radiation measurement, defining the solar and viewing zenith angles (θ_0 and θ, with $\mu_0 = |cos\theta_0|$ and $\mu = |cos\theta|$) and the solar and viewing azimuth angles (φ_0 and φ) towards the zenith in a plane parallel atmosphere. Following the definitions adopted in [RD02], the angles are given at the surface (z = 0m).

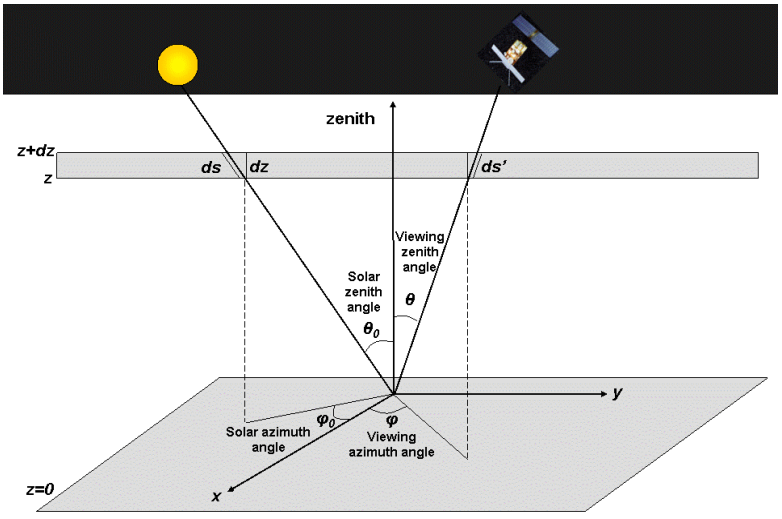

Figure 3: Sketch of satellite radiation measurement and geometry in a plane parallel atmosphere.

The backscattered radiance spectrum recorded by the satellite instrument differs from the solar spectrum because of the interactions of the photons with the Earth's atmosphere and surface reflection. Hence, the radiance spectra contain spectral features that can be related to the various absorbing species and their amounts in the atmosphere. The DOAS method (Platt & Stutz, 2008) aims at the separation of the highly structured trace gas absorption spectra and broadband spectral structures. The technique relies on a number of assumptions that can be summarized as follows:

a. The spectral analysis and atmospheric radiative transfer computations are treated separately by considering one averaged atmospheric light path of the photons traveling from the sun to the instrument.
b. The absorption cross sections are not strongly dependent on pressure and temperature. Additionally, the averaged light path should be weakly dependent on the wavelength – for the fitting window used – which enables defining an effective absorption (slant) column density. Spectrally smoothed structures due broadband absorption, scattering and reflection processes can be well reproduced by a low-order polynomial as a function of wavelength.

The simplification of assuming a single effective light path is valid if the effective light path is reasonably constant over the considered wavelength range.
The spectral analysis in DOAS can be described by the following equation:

$$\ln \frac{I(\lambda)-offset(\lambda)}{E_0(\lambda)} = -\sum_j \sigma_j(\lambda) N s_s + \sum_p c_p \lambda^p \qquad 5\text{-}2$$

where I(λ) is the observed backscattered earthshine radiance [W $m^{-2}nm^{-1}sr^{-1}$], E_0 is the solar irradiance [W $m^{-2}nm^{-1}$]. The first term on the right-hand side indicates all relevant absorbing species with absorption cross-sections $\boldsymbol{\sigma_j}$ [cm^2 $molec.^{-1}$]. Integration of the number densities of these species along the effective light path gives the slant column density $\boldsymbol{Ns_j}$ [$molec.cm^{-2}$]. The second term in Eq. 2 is the polynomial representing broadband absorption and (Rayleigh and Mie) scattering structures in the observed spectrum and also accounts for possible errors such as uncorrected instrument degradation effects, uncertainties in the radiometric calibration or possible residual (smooth) polarization response effects not accounted for in the level 0-1 processing. Equation 2 can be solved by least-squares fitting techniques (Platt and Stutz, 2008) for the slant column values.

Table 1:. DOAS settings used to retrieve BrO slant columns

Fitting interval	332-359 nm
Cross-sections	BrO: 223 K (Fleischmann et al., 2004) O_3: 223K and 243K with Io correction (Serdyuchenko et al., 2014) Pseudo O_3 cross sections ($\lambda\sigma_{O3}$, σ_{O3}^2) (Puķīte et al., 2010) corrected for Io Ring effect (Chance and Spurr, 1997) HCHO: 298K (Meller and Moortgat, 2000) NO_2: 220K (Vandaele et al., 1998) OClO: 213K (Bogumil et al., 2003) O_2-O_2: 293K (Thalman and Volkamer, 2013)
Polynomial	5^{th} order
Intensity offset correction	Linear offset
Spectrum shift and stretch	Fitted
Spectral spikes removal procedure	Active; described in Richter et al. (2011)
Reference spectrum	Averaged earthshine spectrum in Pacific region (15°S-15°N, 160°E-120°W); separate spectrum for each detector column, based on radiance data on the measurement day or as closely in time as possible when not available.

Apart from the cross-sections for the trace gases of interest, additional fit parameters need to be introduced to account for the effect of several physical phenomena on the fit result. These are the filling-in of Fraunhofer lines due to rotational Ramann scattering (Ring effect) and the need for an intensity offset-correction. As outlined before, in the above it is assumed that for the ensemble of observed photons a single effective light path can be assumed over the adopted wavelength fitting interval. For the observation of (generally small) BrO concentrations at large solar zenith angles this is not necessarily the case. For such long light paths, the large contribution of O_3 absorption may lead to biased retrievals. This may be mitigated by taking the wavelength dependence of the O_3 SCD over the fitting window into account, as will be described in the next section.

The different parts of the DOAS retrieval are detailed in the next subsections and Table 1 gives a summary of settings used to invert BrO slant columns. Note that in Eq. 2, the daily solar irradiance is used as a for the reference spectrum. As a baseline, the TCBRO DOAS retrieval uses as reference spectra daily averaged radiances, selected for each across-track position, in the equatorial Pacific. Generally, for an NRT algorithm, the last valid day can be used to derive the reference spectra, while in an offline version of the algorithm, the current day should be used whenever possible. Based on experiences with OMI, this allows, for example, for

better handling of instrumental artefacts and degradation of the recorded spectra for each detector row. The current version of TCBRO is developed for the treatment of offline (OFFL) data only.

Wavelength interval and cross-sections

The DOAS retrieval technique is in principle applicable to all gases having suitable narrow absorption bands in the UV, visible, or near IR regions. However, the generally low concentrations of these compounds in the atmosphere, and the limited signal-to-noise ratio of the spectrometers, restrict the number of trace gases that can be detected. Many spectral regions contain several interfering absorbers and correlations between absorber cross-sections can sometimes lead to systematic biases in the retrieved slant columns. In general, the correlation between cross-sections decreases if the wavelength interval is extended, but then the assumption of a single effective light path defined for the entire wavelength interval may not be fully satisfied, leading to systematic misfit effects that may also introduce biases in the retrieved slant columns (e.g., Pukīţe et al., 2010). To optimize DOAS retrieval settings, a trade-off has to be found between these effects. In the UV-visible spectral region, the cross-section spectrum of BrO has its strongest bands in the 310-360 nm range (Figure 2). For the short wavelengths in this range, the BrO signal however suffers from a strong increase in Rayleigh scattering and ozone absorption. In practice, this leads to a very small BrO signal in the satellite spectra compared to ozone absorption, especially for tropospheric BrO. Consequently, BrO is traditionally retrieved (for GOME, SCIAMACHY, GOME-2, OMI, TROPOMI) using fitting windows in the 328-360 nm range. In our previous study on GOME-2 retrievals (Theys et al., 2011) and operational processing (Theys et al., 2013, 2015), we have used the fitting range of 332-359 nm. However, recent work on TROPOMI BrO (Seo et al., 2019) suggests the use of an optimal fitting range of 334.6-358 nm. Initial comparisons between TCBRO and data kindly provided by the author of that paper, indicated good agreement between the two datasets when using the same settings (within 10-15%, with the remaining differences attributed to a different treatment of the Ring effect), but a positive offset was found between TCBRO BrO columns and independent datasets. After further sensitivity tests of the fitting window boundaries (Figure 4) it was decided to finally adopt the same fitting window as used for previous sensors: 332-359 nm.

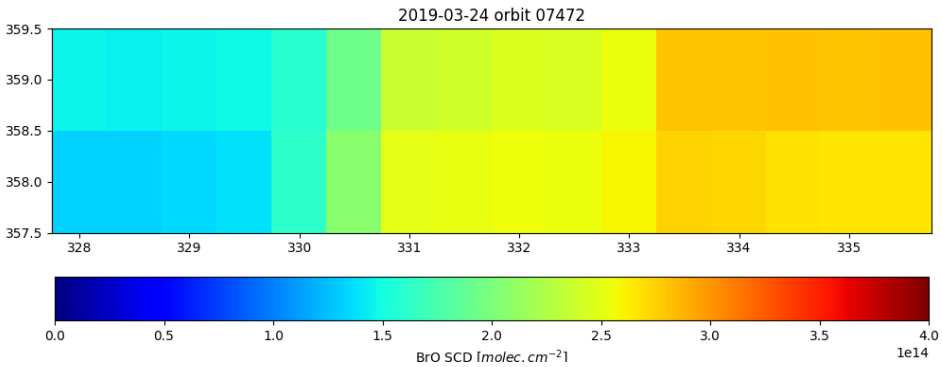

Figure 4: Dependency of the retrieved TCBRO slant column on the boundaries of the wavelength fitting window during a bromine explosion phase on 24 March 2019. Values are averaged over an Arctic region of [70°,75°] latitude and [140°,180°] longitude. The lower boundary was varied between 328 and 335.5 nm. The upper boundary was varied between 358 and 359 nm. In particular, the extension of the lower fitting window boundary to smaller wavelength shows a negative gradient of the retrieved slant column.

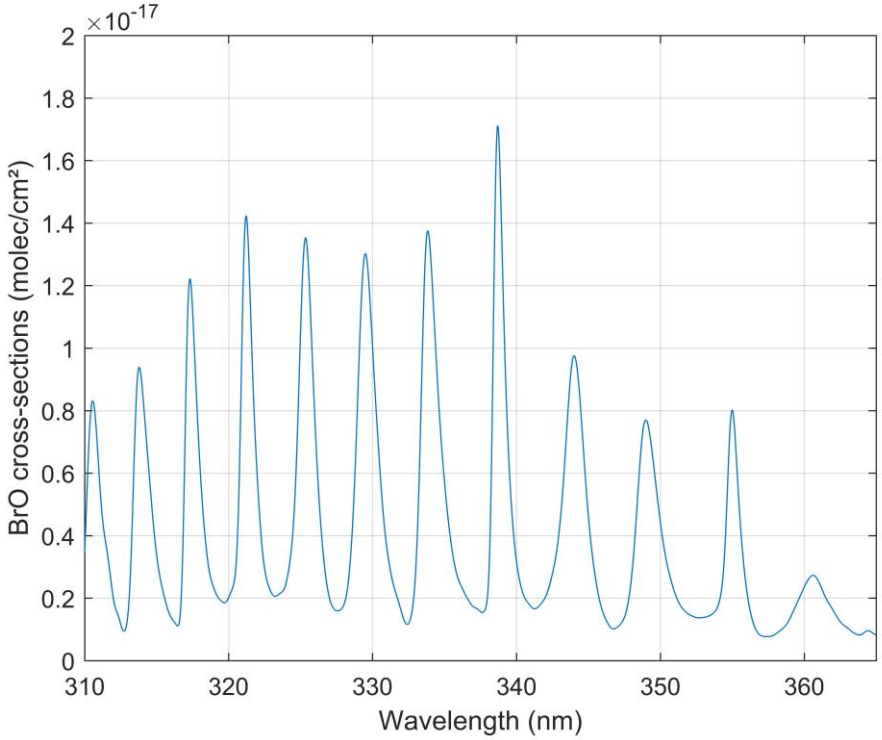

Figure 5: BrO cross-section in the UV convolved at the approximate resolution of S5-P.

Reference radiance database

In its default way of operation, the DOAS fitting procedure requires the measured radiances to be normalized by a reference irradiance spectrum. As mentioned before, it is also common, for the retrieval of atmospheric species, to normalize them by another reference Earthshine spectrum taken in a remote region with expected low concentration levels of the species of interest in order to reduce systematic errors from spectral interferences and/or instrumental limitations. For imager-type of instruments like S5-P, one different reference mean radiance is used for every detector column in order to limit as much as possible stripes originating from imperfect cross-calibration and from different dead/hot pixel masks in different regions of the CCD.
The reference radiance spectra are generated for each detector column separately by averaging as many radiance spectra as possible geo-located within the equatorial Pacific sector (Latitudes: [-15° 15°], Longitudes: [160°E-120°W]). In order to have reference spectra available for the current day, those are calculated by a dedicated auxiliary processor, called BGBRO (background BrO), that is operated independently from TCBRO This auxiliary processor is also responsible for the generation of data for equatorial offset correction (see Section 5.1.2). For technical details regarding BGBRO, see [RD19] and [RD20].

During the slant column fitting procedure, the TCBRO software will ingest the radiance reference data for the current day, when available, or data for a data as closely as possible to the current date. The actual reported reference data is reported in the TCBRO output file.

Wavelength calibration and convolution to S5-P resolution

The quality of a DOAS fit critically depends on the accuracy of the alignment between the earthshine radiance spectrum, the reference spectrum and the cross-sections. Although the Level 1b will contain a spectral assignment, an additional spectral calibration is part of the BrO algorithm.

Moreover, the DOAS spectral analysis includes also the fit of shift and stretch of radiance spectra because the S5-P spectral registration will differ from one ground-pixel to another e.g. due to thermal variations over the orbit as well as due to inhomogeneous filling of the slit in flight direction.

Description of the QDOAS approach to wavelength calibration:

0. Starting point: irradiance and radiance spectra given on their own wavelength grid (those assigned by the level 0-1 processor). For imaging systems like S5-P, each detector column is treated separately as a different instrument.

1. Regridding of the radiance: the radiance spectrum is interpolated on the irradiance (cubic spline), so that both spectra are given on the same wavelength grid

2. Kurucz wavelength calibration: a procedure using the solar Frauhnofer lines from an external reference solar atlas (Chance and Kurucz, 2010) is applied to optimize the wavelength calibration of the solar irradiance. This reference solar spectrum is accurate in absolute vacuum wavelength to better than 0.001 nm and is degraded at the resolution of the instrument, through convolution by the instrumental slit function (ISRF). This procedure uses contiguous sub-windows of approximately 10 nm width each, which allows to compensate for shift and stretch effects. For BrO, 5 sub-windows are used covering the 325-370 nm wavelength range. This step is performed on the solar irradiance for 2 main reasons:

- **i.** The alignment with the solar reference atlas has best accuracy because solar lines are not distorted by atmospheric effects (e.g. due to molecular absorption or Ring effect)
- **ii.** The calibration procedure (which can be relatively heavy if ISRF parameters are also fitted) has to be performed only once per orbit

In practice, wavelength shift and stretch between the reference solar atlas (convolved with S5-P ISRF) and solar irradiance are determined for each sub-window using a non-linear least-squares approach. A polynomial is then fitted through the individual wavelength shifts (for the 4 sub-windows) in order to reconstruct an accurate wavelength calibration for the complete analysis interval.

3. Cross-section gridding: Absorption cross-sections convolved with S5-P ISRF are interpolated (cubic spline) on the optimized wavelength grid of the irradiance

4. DOAS fit: shift and stretch parameters (applied to the radiance) are fitted to properly align all spectral items (irradiance, cross-sections and radiance).

<u>Special case of Earthshine radiances used as reference (rad-as-ref):</u>
An additional step is introduced between step 2 and step 3:

2b. The selected mean earthshine radiance is aligned on the solar irradiance by means of a DOAS fit on the complete wavelength range (325-365 nm in this case), and the shift and stretch values determined in this procedure are used to recalculate the wavelength grid corresponding to the selected rad-as-ref. This wavelength grid becomes the reference grid, and all cross-sections are interpolated on it. Then the analysis proceeds in the same way, using rad-as-ref instead of the solar irradiance. Note that this approach is more accurate than applying the Kurucz calibration directly to the mean radiance, because the alignment (through the DOAS procedure) between two spectra acquired with the same instrument is extremely accurate, and (as already mentioned) the Kurucz procedure (making use of an external solar line reference) has best accuracy when applied to a solar irradiance

Spike removal algorithm

A method to remove individual hot pixels or detector pixels affected by the South Atlantic Anomaly has been demonstrated for NO_2 retrievals in Richter et al. (2011). Often only a few individual detector pixels are affected and in these cases, it is possible to identify and remove the noisy points from the fit. However, as the amplitude of the distortion is usually only of the order of a few percent or less, it cannot always be found in the highly structured spectra themselves. Higher sensitivity for spikes can be achieved by analysing the residual of the fit where the contribution of the Fraunhofer lines, scattering, and absorption is already removed.

When the residual for a single detector pixel exceeds the average residual of all detector pixels by a chosen threshold ratio (the tolerance factor), the pixel is excluded from the analysis, in an iterative process. This procedure is repeated until no further outliers are identified, or until the maximum number of iterations is reached (here fixed to 3). This is especially important to handle the degradation of 2-D detector arrays such as OMI, TROPOMI or the future S4 and S5. However, this improvement of the algorithm has a non-negligible impact on the time of processing. Test retrievals have been done on OMI spectra using a tolerance factor of 5, and a limit of 3 iterations (this could be relaxed) and this leads to an increase in processing time by a factor of 1.5. The settings for the TCBRO algorithm will be determined once all other configuration parameters have been fixed.

Intensity offset-correction

To account for possible stray-light contamination, an intensity offset is subtracted from the measured radiances (Eq. 2). Under the assumption that the intensity offset is rather small compared to the back-scattered intensity, Eq. 2 can be linearized and lead to the fitting of an effective spectrum =offset(λ)/I(λ) in the DOAS analysis. In practice, results of similar quality are found if one fits offset(λ)/E_0(λ) instead of offset(λ)/I(λ). We will use this approach as it is significantly improves the performance with regards to the computation time (the inversion matrix has to be recalculated for each pixel using radiance intensity while it is calculated only once per orbit if the irradiance spectrum is used). As a baseline, the offset(λ) parameter is approximated by a 2nd order polynomial (hence 3 fitting parameters).

Solar-I_0 correction

The DOAS technique assumes a direct linear relationship between the optical depth of a given trace gas and the corresponding cross-section (convolved with the ISRF); the factor between the two being the (retrieved) SCD. In practice, this assumption is not strictly true because there is a difference (known as the solar-Io effect) between cross-sections measured in the laboratory with a smooth light source and the atmospheric absorption measured by an instrument of lower resolution with a structured solar light source. A commonly accepted approach to treat the solar-Io effect is to correct the cross-sections for this effect (mostly O_3 cross-sections need to be corrected):

$$\boldsymbol{\sigma_{Io-corr}} = -\frac{\mathbf{1}}{\boldsymbol{SC}} . \boldsymbol{ln}\left[\frac{\boldsymbol{F*(Io.\exp\left(-SC.\sigma(\lambda)\right))}}{\boldsymbol{F*Io}}\right] \qquad 5\text{-}3$$

where F is the instrumental slit function, Io is a high resolution solar spectrum, σ is the high resolution O_3 cross-section and SC is a typical O_3 slant column density. SC is often assumed to be constant over the fitting interval but in the short UV, this approximation is not valid, because the O_3 AMF is wavelength dependent. If one considers a first order Taylor expansion of the ozone optical depth, the wavelength dependence of the AMF can be expressed as in Pukite et al., 2010: ς(λ)=P_1λ+P_2σ and the equation can be linearized and expressed as : $\boldsymbol{\tau = SC_{O3}.\sigma_{Io-corr} + \frac{F*(Io.\exp(-SCo.\sigma(\lambda)).\varrho(\lambda).\sigma(\lambda)))}{F*(Io.\exp(-SCo.\sigma(\lambda)))}}$, where $\boldsymbol{\sigma_{Io-corr}}$is the solar-Io corrected O_3 cross-section; SC_{O3} is a corresponding parameter that is different from the assumed zero-order ozone slant column SCo. Injecting the formulation of Pukite et al. (2010), two new terms are found (Pukite terms corrected for solar Io):

$$\boldsymbol{Puk1_{Io-corr}} = \frac{\boldsymbol{F*(Io.\exp\left(-SCo.\sigma(\lambda)\right).\lambda.\sigma(\lambda)))}}{\boldsymbol{F*(Io.\exp\left(-SCo.\sigma(\lambda)\right))}}$$

$$\boldsymbol{Puk2_{Io-corr}} = \frac{\boldsymbol{F*(Io.\exp\left(-SCo.\sigma(\lambda)\right).\sigma(\lambda)^2))}}{\boldsymbol{F*(Io.\exp\left(-SCo.\sigma(\lambda)\right))}} \qquad 5\text{-}4$$

5.1.2 Equatorial offset correction

Even if the use of averaged earthshine spectra as reference spectra is an efficient way of reducing offsets, across-track striping can possibly arise, due to imperfect cross-calibration and different dead/hot pixel masks

for the CCD detector regions. Therefore, an offset correction is needed also to compensate for the residual BrO slant column in the reference spectra (mostly of stratospheric origin) and to handle the possible time-dependent degradation of the instrument (e.g. strongly showing up during the advanced lifetime of GOME-2A and now also in GOME-2B)
In practice, an equatorial offset correction is applied on a daily basis to the BrO data (Richter et al., 2002), separately for each of the cross-track position. For this, averaged BrO slant columns in the tropical latitudinal band between ±15° are calculated on a daily basis, assuming small equatorial BrO columns with no significant seasonal variations. These averaged slant columns are then subtracted from all slant columns. Finally, assuming a constant equatorial background VCD of 3.5 x 10^{13} molec/cm² () and taking the variation of the viewing angle (VZA) over the swath into account, a background component is added to the derived slant column.

Experience with TROPOMI operational processing indicates that a proper handling of the offset correction is important. In particular a fall-back correction should be available at any time in case of data gap/ interruption of nominal radiance measurements (e.g. due to calibration period). If no data is found for the current day, a fallback is used instead, that is the last valid offset correction data (updated on a daily basis). The offset correction data is produced by the auxiliary BGBRO processor and data close to the current data should normally available.

5.1.3 AMF and VCD determination

The next step in the BrO column algorithm is the calculation of the total vertical column density N_v.

In the current verson of the algorithm. for the total BrO column derivation a geometric air mass factor is applied. For the stratospheric part of the BrO profile, such a geometric AMF is generally close to the real AMF. Realising that there is also a tropospheric component of the total BrO column, the motivation to use a geometric AMF to derive the total column is twofold:

- The true, altitude dependent AMF profile is strongly influenced by the surface reflectance. For high albedo values the true AMF is close to the geometric approximation also for low altidudes. Such high albedo values occur with snow/ice surfaces, found in region where high BrO values in spring are encountered.
- Indications exist for substantial BrO amounts in the free troposphere. Here the geometric AMF approach is generally reasonable, also for low-reflecting surfaces.

The treatment of the AMF may be revised in future updates of this algorithm.

The geometric AMF is expressed as:

$$\frac{1}{\cos\theta} + \frac{\sqrt{(\cos\theta_0)^2+\varepsilon^2+2\varepsilon}-\cos\theta}{\varepsilon} \qquad 5\text{-}5$$

Where ε=60./R_E, with R_E the radius of the Earth and Θ_0 and Θ are the solar zenith angle and viewing zenith angle, respectively.

5.2 Error Analyses

The total uncertainty (trueness and precision) on the retrieved BrO columns derives from a wide range of error sources. In part, those are related to the measuring instrument, such as uncertainties due to noise or knowledge of the slit function. In the retrieval algorithm, those instrumental errors propagate into the uncertainty on the slant column. Other types of error can be considered as model errors and are related to the representation of physical properties that are not directly measured from the spectrum. Examples of model errors are uncertainties in the trace gas absorption cross-sections, the treatment of clouds and uncertainties of the a priori profile. Model errors can affect both the slant column results and the air mass factor.

A formulation of the error can be derived analytically by error propagation, starting from the equation of the vertical column (4-1) which directly results from the different retrieval steps. As the main algorithm steps are

performed independently, they are assumed to be uncorrelated. If we further assume normal probability distributions, the total error on the tropospheric vertical column can be expressed as (Boersma et al., 2004, De Smedt et al., 2008):

$$\sigma_{N,v}{}^2 = \frac{1}{M^2}\left(\sigma_{N,s}{}^2 + \frac{(\Delta N_S + M_0 N_{v,0})^2}{M^2}\sigma_M{}^2 + \sigma_{N,s,0}{}^2 + N_{v,0}{}^2\sigma_{M,0}{}^2 + M_0{}^2\sigma_{N,v}{}^2\right) \quad 5\text{-}6$$

where $\sigma_{N,s}$, σ_M, $\sigma_{N,s,0}$, $\sigma_{M,0}$ and $\sigma_{N,v,0,CTM}$ are respectively the errors on the slant column, the air mass factor, and the slant column correction, the air mass factor, and the model vertical column in the reference sector (indicated by suffix 0).

A difficulty in DOAS error formulation comes from the fact that it generally assumes the different error sources of the algorithm to be independent and uncorrelated, which is not strictly valid. For example, the background correction is designed to overcome systematic features/deficiencies of the slant column fitting and these two steps cannot be considered as independent. Hence, summing up all the corresponding error estimates would lead to overestimated error bars.

Another important point to note is that, in principle, systematic and random components of each given error source should be discriminated. If so, when deriving the error on the BrO vertical column, each of the components of (**5-6**) can be written as:

$$\sigma_k^2 = \frac{\sigma_{k,rand}^2}{N} + \sigma_{k,syst}^2 \quad 5\text{-}7$$

where N is the number of ground pixels considered when averaging the observations. It is however very complicated to separate them in practice (see for example Boersma et al., 2004).

5.2.1 Contributions to the error in the slant column

Error sources that contribute to the total uncertainty on the slant column originate both from instrument characteristics and from uncertainties in the DOAS slant column fitting procedure itself.

5.2.1.1 Random errors on slant columns

The retrieval noise for individual observations is limited by the SNR of the spectrometer measurements. A good estimate of the random error variance of the reflectance (which results from the combined noise of radiance and reference spectra) is given by the reduced χ^2 of the fit, which is defined as the sum of squares divided by the number of degrees of freedom in the fit. The covariance matrix (Σ) of the linear least squares parameter estimate is then:

$$\Sigma = \frac{\chi^2}{(k-n)}(A^T A)^{-1} \quad 5\text{-}8$$

where k is the number of spectral pixels in the fitting interval, n is the number of parameters to fit and the matrix $A(jxk)$ is formed by the absorption cross-sections. For each absorber j, the value $\sigma_{N_{s,j}}$ is usually called the slant column error (SCE or $\sigma_{N_s,rand}$).

$$\sigma_{N,s,j}^2 = \frac{\chi^2}{(k-n)}(A^T A)_{j,j}^{-1} \quad 5\text{-}9$$

For individual satellite ground pixels, the random error on the slant columns is the most important source of error on the total vertical column. It can be reduced by averaging the observations, but of course to the expense of a loss in time and/or spatial resolution. Currently, we adopt this error, coming from the slant column fitting procedure, as the only component contributing to the slant column uncertainty.

5.2.1.2 Systematic errors on the slant columns

Equation (5-8) does not take into account systematic errors, that are mainly dominated by slit function and wavelength calibration uncertainties, absorption cross-section uncertainties, by interferences with other species (O_3, HCHO and O_4), or by stray light corrections. Those contributions to the slant column errors need to be estimated from sensitivity tests and this remains to be done. Until then, the systematic error to the slant column is estimated to be 20% (see Theys et al., 2011).

TBD: Perform sensitivity tests on satellite data to estimate systematic contributions to the slant column uncertainty.

5.2.2 Contributions to the error in the air mass factor

In the current version of the algorithm, a strongly simplified approach is taken. First of all, by using a geometric air mass factor approach ($M = M_{geo}$), all error contributions related to the AMF a set to zero, as no contributions of physical quantities (cloud parameters, surface albedo, …) to the AMF are currently taken into account.

Based on sensitivity studies on the validity of the geometric approach for the AMF, a proper error propagation analysis can be performed. The stratospheric component of the AMF can accurately be described by a geometric AMF and the contribution to the total AMF uncertainty budget can be neglected in most measurement conditions. For the troposphere, the error budget calculations is much more complex.

Until further details on this matter have been investigated, the total AMF uncertainty is estimated from values in literature and is set to 10%.

TBD: Perform sensitivity study into the validity of the geometric approach for the AMF over different scene types.

6 Feasibility

6.1 Estimated computational effort

The Sentinel-5P sensor TROPOMI samples the Earth's surface with an unprecedented spatial resolution of 7.2×3.5 km^2 around nadir, 5.5×3.5 km^2 as of 6 August 2019. Although this allows resolving fine details in the observed products, in comparison to results from previous sensors, it poses additional demands on the retrieval code regarding computational speed.

The Level 1b data flow delivers spectral measurements for band 3 with a size of 2.7 (3.45) gigabytes per orbit. In order to estimate the computational effort, an analysis was made of one month of per-orbit L2 calculations by TCBRO on the S5P-PAL system ([URL05]). Typical numbers for the calculation of one orbit worth of L2 data are given in Table 2.

A significant advantage of the S5P-AL system is the scalability. In case of high relevance, additional compute nodes can be quickly made available.

The numbers reflect the processor version BGBRO 1.2.2 and TCBRO 1.2.3. Earlier processor versions required almost twice as long for the same calculation. The improvement is due to the switch to QDOAS v3.6 (available as conda-forge package) for the calculations of the slant columns.

Table 2 The numbers give an estimate of a typical execution duration. The actual time from submission of the job request to end of execution may be longer, depending on the number of jobs requested simultaneously or the activity of the available compute cores at the moment of submission.

A significant advantage of the S5P-AL system is the scalability. In case of high relevance, additional compute nodes can be quickly made available.

The numbers reflect the processor version BGBRO 1.2.2 and TCBRO 1.2.3. Earlier processor versions required almost twice as long for the same calculation. The improvement is due to the switch to QDOAS v3.6 (available as conda-forge package) for the calculations of the slant columns.

Table 2: Estimates of TCBRO processing times on the S5P-PAL system for one TROPOMI orbit.

	Time for TROPOMI (min)	Software component
Slant column (1 fitting window + spike removal algorithm)	20	QDOAS
AMF	2	
Normalization	3	
Total	25	

Computational cost was also estimated for the auxiliary processor BGBRO. There, the most time consuming component is the calculation of slant column data for the calculation of average BrO concentration over the Pacific reference region. This involves typically 5 orbits and thus takes longer than the single-orbit calculations of TCBRO listed above. On the other hand, the BGBRO executions needs only to be performed once per day.

Table 3: Estimates of TCBRO processing times on the S5P-PAL system for results for one day.

	Execution time on S5P-PAL	Software component
Slant column fitting (1 fitting window + spike removal algorithm)	100	QDOAS
Calculation of average radiance spectrum	25	
Total	125	

6.2 High level data product description

In addition to the main product results, such as the BrO slant column, vertical column and air mass factor, the level 2 data files contain several additional parameters and diagnostic information. Table 4 gives a minimum set of data fields that are present in the Level 2 data. A 1-orbit BrO column Level 2 file is about 147 MB (up to 189 MB from 6 August 2019 onward), including averaging kernels and a priori profile information. More details about the level 2 data format and the of the auxiliary data produced by BGBRO are provided in the Product Format Specification document [RD21].

Table 4: List of principle output fields in the TCBRO BrO product. scanline x ground_pixel mean the number of pixels in an orbit along track and across track, respectively.

Symbol	Unit*	Variable name	Number of entries
N_v	mol.m^{-2}	brominemonoxide_total_vertical_column	scanline x ground_pixel
$N_{s,1}$	mol.m^{-2}	fitted_slant_columns	scanline x ground_pixel x number_of_slant_columns
$\sigma_{N,s,1,rand}$	mol.m^{-2}	fitted_slant_columns_precision	scanline x ground_pixel x number_of_slant_columns
N_s - $N_{s,0}$	mol.m^{-2}	brominemonoxide_slant_column_corrected	scanline x ground_pixel
$N_{v,0}$	mol.m^{-2}	brominemonoxide_total_vertical_column_correction	scanline x ground_pixel
M	n.u.	Bromoniemonoxide_geometric_air_mass_factor	scanline x ground_pixel
$\sigma_{N,v,rand}$	mol.m^{-2}	brominemonoxide_total_vertical_column_precision	scanline x ground_pixel
$\sigma_{N,v,syst}$	mol.m^{-2}	brominemonoxide_total_vertical_column_trueness	scanline x ground_pixel
$\sigma_{N,s,0}$	mol.m^{-2}	formaldehyde_slant_column_corrected_trueness	scanline x ground_pixel

6.3 Auxiliary information needs

The auxiliary data needs listed below are separated into static and dynamic needs.

6.3.1 Dynamic information

See also the TCBRO Input / Output Definition Document [RD19].

Table 5: Dynamic auxiliary information needs in the HCHO retrieval algorithm

Name/Data	Symbol	Unit	Source	Pre-process needs	Backup if not available
S5P level 1B Earth radiance	I	mol.s^{-1}m^{-2}nm^{-1}sr^{-1}	S5P L1b product	-	No retrieval
S5P level 1B sun irradiance	E_0	mol.s^{-1}m^{-2}nm^{-1}	S5P L1b product	Wavelength recalibrated using a high-resolution reference solar spectrum	Use previous measurement
S5P level 2 cloud parameters		n.u.	S5P operational cloud product based on a Lambertian cloud model.	-	Ingested but currently not used

6.3.2 Static information

See also the TCBRO Input / Output Definition Document [RD19].

Table 6: Static auxiliary information needs in the HCHO retrieval algorithm

Name/Data	Symbol	Unit	Source	Pre-process needs	Comments
Absorption cross-sections					
BrO	σ_{BrO}	cm^{2}molec.$^{-1}$	Fleischmann et al. (2004), 223K	Convolution at the instrumental spectral resolution using the provided slit function	-
HCHO	σ_{HCHO}	cm^{2}molec.$^{-1}$	Meller and Moortgat (2000), 298K		
Ozone	σ_{o3223} σ_{o3243}	cm^{2}molec.$^{-1}$	Serdyuchenko et al. (2013), 223 + 243K		
OClO		cm^{2}molec.$^{-1}$	Bogumil et al. (2003), 213 K		
NO_2	σ_{NO2}	cm^{2}molec.$^{-1}$	Vandaele et al. (1998), 220K		
O_4 (O_2-O_2)	σ_{O4}	cm^{5}molec.$^{-2}$	Thalman et al., 2013, 293K		
High resolution reference	E_s	W m^{-2}nm^{-1}	Chance and Kurucz, 2010	-	-

solar spectrum					
Ring effect	$\sigma_{ringev1}$ $\sigma_{ringev2}$	$cm^2molec.^{-1}$	2 Ring cross-sections generated internally.	A high-resolution reference solar spectrum and the instrument slit function are needed to generate the data set.	Calculated in an ozone containing atmosphere for low and high SZA, using LIDORT_RRS (Spurr et al., 2008b) and a standard atmosphere (Camelot European Pollution atmospheric profile).
Non-linear O_3 absorption effect	σ_{o3l} σ_{o3sq}	$nm.cm^2molec.^{-1}$ $cm^4molec.^{-2}$	2 pseudo-cross sections generated internally.	The O_3 cross-section at 223 K is needed.	Calculated from the Taylor expansion of the wavelength and the O_3 optical depth (Puķīte et al., 2010).
Instrument slit function	SF	n.u.	Slit Function per wavelength/detector.	-	Values between 325 and 360nm.

7 Validation

Based on one year of BrO VCD L2 data generated by TCBRO, comparisons with ground-based zenith-sky measurements over Harestua (Norway) have been performed, as well as comparisons with data from the GOME-2 instruments on the MetOp-B and –C platforms. A detailed description of these exercises can be found in [RD18] . Here, the main results are repeated.

Although refinements to the TCBRO algorithm are still required, first comparisons with external datasets have been performed as a first assessment of the quality of the L2 results.Those exercises are briefly described below. Further details can be found in [RD18].

7.1 Comparison with ground-based DOAS BrO data.

The « Solobservatoriet of Harestua » is a small but well-known solar observatory near Harestua, located about 40 km northwards of Oslo, Norway. Harestua is part of the NDACC network as a complementary station. BIRA-IASB operates a fully automated zenith-sky DOAS instruments since 1998 and provides the NDACC data base with stratospheric NO_2, O_3, BrO and OClO data.

Here, we compare one year (2019) of Harestua zenith-sky BrO data (March-May 2019) with daily-averaged TCBRO columns. The results are shown in Figure 6.

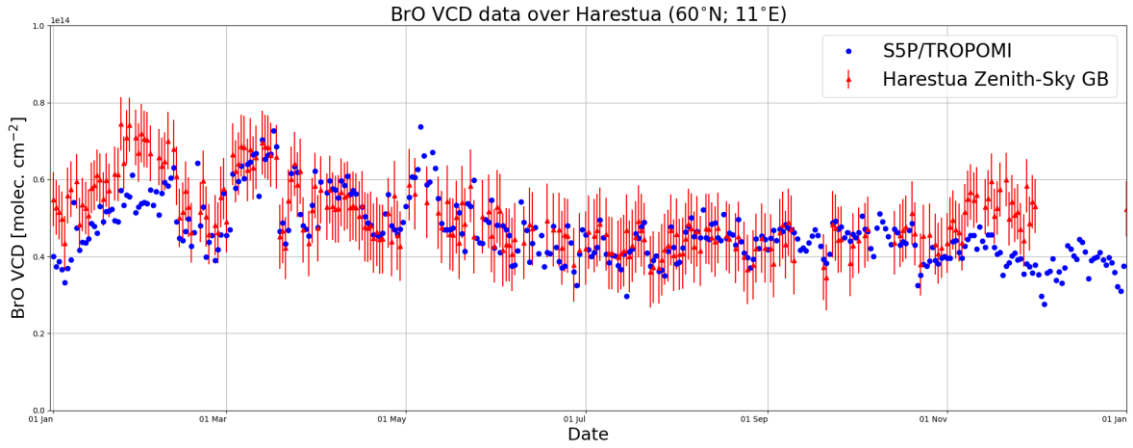

Figure 6: Daily BrO vertical column data as measured from Harestua (**red**) and with TROPOMI (**blue**). The two datasets agree well for the period March-October 2019, ut sow larger differences in wintertime.

The retrieved columns follow the time variation of the ground-based data very well, but show a negative bias over the winter months. Probably, this is due to less accurate AMF values in the TCBRO results; A similar negative bias was observed earlier for GOME-2B and –C BrO VCD's, that where obtained by using an AMF based on a purely stratospheric profile (Merlaud et al., 2020).

7.2 Comparison with other satellite platforms

A comparison of the same TROPOMI BrO columns with GOME-2 data shows larger differences. These comparisons where made based on monthly averaged values for 12 overpass stations at different latitudes. Results for two of these stations are depicted in Figure 7. The TCBRO results agree quite well with the GOME-2 measurements but show a positive bias of about 1×10^{13} molec cm^{-2}. More comparisons with round-based measurements at other locations than Harestua would help with the interpretations of these differences.

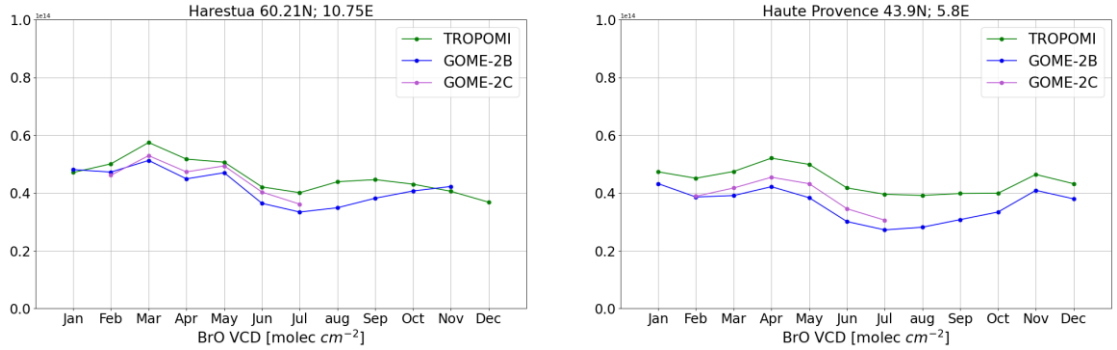

Figure 7: Comparison of monthly averaged TCBRO BrO VCD's with equivalent data from GOME-2B and –C, for two of the twelve investigated overpass overpass stations. The TCBRO columns show a positive offset of about 1×10^{13} molec cm^{-2} with respect to the GOME-2 data.

8 Final words

This document presents the current status of the BIRA-IASB Bromine Monoxide total vertical column algorithm TCBRO. The retrieval algorithm for the TROPOMI BrO product generation is based on the heritage from algorithms successfully developed for the SCIAMACHY, GOME-2, and OMI sensors. Based on literature and sensitivity studies, a fitting wavelength window of 332.0 – 359.0 nm has been selected, corresponding to the wavelength range already in use for heritage sensors.
Earthshine radiance averaged in the remote Pacific are used as reference for the DOAS fit. Spectral outlier screening is applied during the fitting procedure (spike removal algorithm). The BrO retrieval algorithm also includes a post-processing across-track reference sector correction, to minimize striping effects.
The details of the DOAS-type algorithm have been outlined in the document at hand and first comparisons with reference data sets have been performed. The latter show good agreement with reference data, although further comparisons would likely increase the understanding of the differences that remain.

Although first estimates on the product uncertainty information, a proper error propagation analysis needs still to be performed and better uncertainty estimates are expected in a future update. The validity of the use of a geometric air mass factor will then also be better understood and it may be decided to turn more advanced AMF calculation methods.

References

Boersma, K. F., Eskes, H. J. and Brinksma, E. J.: Error analysis for tropospheric NO2 retrieval from space, J. Geophys. Res., 109(D4), doi:10.1029/2003JD003962, 2004.

Bogumil, K., Orphal, J., Homann, T., Voigt, S., Spietz, P., Fleischmann, O.C., Vogel, A., Hartmann, M., Bovensmann, H., Frerick, J., and Burrows, J.P., Measurements of molecular absorption spectra with the SCIAMACHY pre-flight model: Instrument characterization and reference data for atmospheric remote sensing in the 230-2380 nm region, J. Photochem. Photobiol. A: Chem. 157, 167-184 (2003); DOI: 10.1016/S1010-6030(03)00062-5

Chance, K. and R. J. Spurr: Ring effect studies: Rayleigh scattering including molecular parameters for rotational Raman scattering, and the Fraunhofer spectrum, Applied Optics, 36, 5224-5230, 1997.

Chance, K. V., Palmer, P. I., Martin, R. V., Spurr, R. J. D., Kurosu, T. P. and Jacob, D. J.: Satellite observations of formaldehyde over North America from GOME, Geophysical Research Letters, 27(21), 3461-3464, doi:10.1029/2000GL011857, 2000.

Chance, K. and Kurucz, R. L.: An improved high-resolution solar reference spectrum for earth's atmosphere measurements in the ultraviolet, visible, and near infrared, J. Quant. Spectrosc. Radiat. Transf., 111(9), 1289-1295, 2010.

De Smedt, I., Müller, J.-F., Stavrakou, T., van der A, R., Eskes, H. and Van Roozendael, M.: Twelve years of global observations of formaldehyde in the troposphere using GOME and SCIAMACHY sensors, Atmos. Chem. Phys., 8(16), 4947-4963, 2008Fayt, C. and M. Van Roozendael: Windoas 2.1, Software User Manual, BIRA-IASB, 2001.

Danckaert, T., Fayt, C., Van Roozendael, M., De Smedt, I., Letocart, V., Merlaud, A., Pinardi, G: Qdoas Software User Manual, Version 2.1, http://uv-vis.aeronomie.be/software/QDOAS/QDOAS_manual_2.1_201212.pdf, 2012.

Fehr, T.: Sentinel-5 Precursor Scientific Validation Implementation Plan, EOP-SM/2993/TF-tf, 1.0, http://doi.org/10.5281/zenodo.165739, 2016.

Fleischmann, O. C., et al. : New ultraviolet absorption cross-sections of BrO at atmospheric temperatures measured by time-windowing Fourier transform spectroscopy, J. Photochem. Photobiol. A, 168, 117–132, 2004.

Meller, R., and Moortgat, G. K.: Temperature dependence of the absorption cross section of HCHO between 223 and 323K in the wavelength range 225–375 nm, J. Geophys. Res., 105(D6), 7089–7102, doi:10.1029/1999JD901074, 2000.

Merlaud, A., Theys, N., Hendrick, F., Van Gent, J., Pinardi, G,. Van Roozendael, M., Chan, K. L., Heue, K. P., and Valks, P.: Validation report of GOME-2 GDP 4.9 BrO column data for MetOp-C Operational Readiness Review, AC-SAF Validation Report, version 1.1, 19 May 2020, https://acsaf.org/docs/vr/Validation_Report_OTO_BrO_May_2020.pdf

Platt, U.: Differential optical absorption spectroscopy (DOAS), in Air Monitoring by Spectroscopic Techniques, M.W. Sigrist ed., Chemical Analysis Series, Wiley, New York, 127, 27-84, 1994.

Platt, U and Stutz, J.: Differential Optical Absorption Spectroscopy: Principles and Applications (Physics of Earth and Space Environments), Springer-Verlag, Berlin, Heidelberg, ISBN 978-3540211938, 2008.

Puķīte, J., Kühl, S., Deutschmann, T., Platt, U., and Wagner, T.: Extending differential optical absorption spectroscopy for limb measurements in the UV, Atmos. Meas. Tech., 3, 631-653, 2010.

Richter, A , F. Wittrock, M. Eisinger and J. P. Burrows (1998), GOME observations of tropospheric BrO in Northern Hemispheric spring and summer 1997, Geophys. Res. Lett., No. 25, pp. 2683-2686.

Richter, A., Wittrock, F., Ladstätter-Weissenmayer, A., and Burrows, J. P. (2002), GOME measurements of stratospheric and tropospheric BrO, Adv. Space Res., 29, 1667-1672.

Richter, A., Begoin, M., Hilboll, A. and Burrows, J. P.: An improved NO2 retrieval for the GOME-2 satellite instrument, Atmos. Meas. Tech., 4(6), 213-246, doi:10.5194/amt-4-1147-2011, 2011.

Seo, S., Richter, A., Blechschmidt, A.-M., Bougoudis, I., and Burrows, J. P.: First high-resolution BrO column retrievals from TROPOMI, Atmos. Meas. Tech., 12, 2913–2932, https://doi.org/10.5194/amt-12-2913-2019, 2019.

Serdyuchenko, A., Gorshelev, V., Weber, M., Chehade, W., and Burrows, J. P.: High spectral resolution ozone absorption cross-sections – Part 2: Temperature dependence, Atmos. Meas. Tech., 7, 625-636, doi:10.5194/amt-7-625-2014, 2014.

Thalman, R. and Volkamer, R.: Temperature dependent absorption cross-sections of O2-O2 collision pairs between 340 and 630 nm and at atmospherically relevant pressure., Phys. Chem. Chem. Phys., 15(37), 15371–81, doi:10.1039/c3cp50968k, 2013.

Theys, N., Van Roozendael, M., Hendrick, F., Yang, X., De Smedt, I., Richter, A., Begoin, M., Errera, Q., Johnston, P. V., Kreher, K., and De Mazière, M.: Global observations of tropospheric BrO columns using GOME-2 satellite data, Atmos. Chem. Phys., 11, 1791–1811, https://doi.org/10.5194/acp-11-1791-2011, 2011.

Vandaele A.C., C. Hermans, P.C. Simon, M. Carleer, R. Colin, S. Fally, M.F. Mérienne, A. Jenouvrier, and B. Coquart, Measurements of the NO2 absorption cross-section from 42000 cm-1 to 10000 cm-1 (238-1000 nm) at 220 K and 294 K, J.Q.S.R.T., 59, 171-184, 1998.

Van Roozendael, M., V. Soebijanta, C. Fayt, and J.-C. Lambert: Investigation of DOAS Issues Affecting the Accuracy of the GDP Version 3.0 Total Ozone Product, in ERS-2 GOME GDP 3.0 Implementation and Delta Validation, ERSE-DTEX-EOAD-TN-02-0006, ESA/ESRIN, Frascati, Italy, Chap.6, pp.97-129, 2002.